Cell Division

RESEARCH

Open Access

RFX2 downregulates RASSF1 expression and YAP phosphorylation through Hippo signaling to promote immune escape in lung adenocarcinoma

Zhenzhen Kong[1,2†], Ping Zhou[3†], Jiahao Xu[1,2], Ying Zhang[1,2] and Yong Wang[1,2*]

Abstract

Objective Regulatory Factor X (RFX) transcription factors have been implicated in different cancers. Ras association domain family (RASSF) has been shown clinical significance in lung cancer. This paper was to investigate the interaction of RFX2 and RASSF1 in lung adenocarcinoma (LUAD).

Methods The transcriptome differences of LUAD patients in GSE32863, GSE43458, and GSE21933 datasets were analyzed. A-549 and NCI-H358 cell lines after overexpression of RFX2 were co-cultured with activated $CD8^+$ T cells, and the release of IFN-γ, GZMB, PRF1 by $CD8^+$ T cells, and PD-L1 in the LUAD cells were detected. Cell viability, invasion, and apoptosis were analyzed by CCK-8, Transwell, and TUNEL assays. Dual-luciferase assay and ChIP were conducted to detect the interaction between RFX2 and RASSF1 promoter. An in vivo tumor model was constructed to monitor tumor growth. YAP protein levels and phosphorylation were measured. A-549 and NCI-H358 cells treated with DMSO or PY-60 after RFX2 overexpression were co-cultured with activated $CD8^+$ T cells.

Results RFX2 was notably downregulated in LUAD. RFX2 overexpression increased infiltrating $CD8^+$ T cells within transplanted tumors and inhibited immune escape, proliferation, and invasion of LUAD cells. RFX2 was enriched in the RASSF1 promoter, and RFX2 activated RASSF1 transcription by binding to the RASSF1 promoter. RASSF1 knockdown reversed the ability of RFX2 overexpression to inhibit immune escape. RFX2 depletion downregulated RASSF1, which reduced YAP phosphorylation, thus affecting the Hippo pathway to promote the immune escape.

Conclusion RFX2 Loss in LUAD downregulates RASSF1 expression and YAP phosphorylation, thereby promoting immune escape through Hippo signaling.

Keywords RFX2, Lung adenocarcinoma, RASSF1, Hippo signaling pathway, Immune escape

†Zhenzhen Kong and Ping Zhou have contributed equally to this work.

*Correspondence:
Yong Wang
wyong827@163.com
Full list of author information is available at the end of the article

Introduction

Despite continued efforts into the screening and treatment of lung cancer, it remains one of the most common causes of cancer death worldwide and lung adenocarcinoma (LUAD) is its most common histological subtype, with most of its cases found at advanced stages [1]. The 5-year survival rate is about 55% for localized lung cancer, in contrast to only 5% for distant spread [2]. LUAD also shows strong resistance to conventional radiotherapy and chemotherapy, which poses a great challenge to effective treatment [3]. The intrinsic and acquired resistance of LUAD is closely associated with the tumor immune microenvironment, in which cancer cells induce immune escape and evade immune surveillance [4]. Like other subtypes of lung cancer, LUAD can hijack and evade host immune surveillance mechanisms, highlighting the importance of understanding the cross-talk between the developing tumors and the immune cells [5]. Therefore, upgrading the limited response rate to immunotherapy might be an option to improve the prognosis for patients with late-stage non-small cell lung cancer (NSCLC).

Public GEO databases show that regulatory factor X 2 (RFX2) is among the 21 differentially expressed genes (DEGs) in LUAD. RFX transcription factors are defined by a conserved, specialized winged-helix type DNA-binding domain and can regulate genes involved in the cell cycle and the functional maturation of cells of the immune response [6]. RFX2 is a transcription factor or gene expression regulator that is abundantly expressed in advanced LUAD [7]. Additionally, RFX2 has been identified as one of the top three master transcription factors in regulating angiogenesis signature in patients with kidney renal clear cell carcinoma [8]. However, further knowledge about the implication of RFX2 in LUAD is insufficient.

More than 30% of cancers have shown Ras gene mutation and the Ras association domain family (RASSF), among which RASSF1 to RASSF6 is referred to as the C-RASSF proteins, can facilitate activated Ras-mediated cell death [9]. RASSF1 is an important tumor suppressor and its hypermethylation is another frequent event in lung cancer affecting approximately 60% of LUAD [10]. A previous study revealed that activating the Hippo pathway via RASSF1 by ursolic acid suppresses the tumorigenesis of gastric cancer [11]. The Hippo pathway is considered to be in the active state when the MST and LATS kinases are active, and the activated LATS1/2 in turn phosphorylates their downstream targets YAP and TAZ, contributing to these two transcriptional co-activators in their nuclear export, cytoplasmic retention and/or proteasomal degradation [12]. More importantly, YAP nuclear localization and/or total YAP expression are correlated with PD-L1 expression in human NSCLC tissues [13]. Nevertheless, we know little about the role of RASSF1 and its interaction with the Hippo pathway on LUAD. This study aims to reveal the effects of RXF2 on LUAD evading immune system surveillance and defense via RASSF1 and corresponding molecular mechanism of action.

Results

Differential expression of RFX2 in LUAD

To further investigate the molecular mechanisms of NSCLC progression and immune escape, DEGs between 21 cases of NSCLC tissues and paired normal lung tissues in the GSE21933 dataset (Fig. 1A), between LUAD tissue of 80 LUAD patients and normal lung tissue of 30 never-smoker cases in the GSE43458 dataset (Fig. 1B), and 58 LUAD and 58 adjacent non-tumor lung fresh frozen tissues in the GSE32863 dataset were analyzed (Fig. 1C) through the public GEO database with Benjamini & Hochberg (False discovery rate) and p adj < 1e-05 as the screening condition. The top 2500 DEGs in LUAD were downloaded from GEPIA (http://gepia.cancer-pku.cn/index.html) in order of p adj from smallest to largest. Then human transcription factors were downloaded from HumanTFDB (http://bioinfo.life.hust.edu.cn/HumanTFDB#!/). The DEGs in the GSE32863, GSE43458, and GSE21933 datasets and the first 2500 DEGs of LUAD in GEPIA and human TFs were screened with the threshold of P adj < 1e-05. Subsequently, 21 intersections were obtained via Jvenn (https://jvenn.toulouse.inrae.fr/app/example.html) (Fig. 1D). The prognostic significance of 21 genes in lung cancer was subsequently analyzed in Kaplan–Meier Plotter (http://kmplot.com/analysis/index.php?p=background) (Fig. S1). From the log-rank P-value, TGT3 (FOXM1) showed the greatest difference in prognostic significance. Since FOXM1 is well-known in cancers, particularly lung cancer [14, 15], we excluded it and instead focused on RFX2, which was the second in prognostic significance. Lung cancer patients with significantly low RFX2 expression had significantly poorer overall survival (OS), which echoed the significantly low expression of RFX2 in datasets GSE32863 (LogFC = − 0.43), GSE43458 (LogFC = − 1.0663699), and GSE21933 (LogFC = − 2.030599) (Supplementary Material).

Next, 36 specimens from LUAD patients and their corresponding adjacent normal tissues were analyzed by immunohistochemical (IHC) staining. IHC staining showed that RFX2 was markedly attenuated in LUAD tissues compared with normal tissues (Fig. 1E). RT-qPCR showed that the mRNA expression of RFX2 in LUAD tissues was greatly lower than that in adjacent normal tissues (Fig. 1F). In brief, RFX2 is significantly

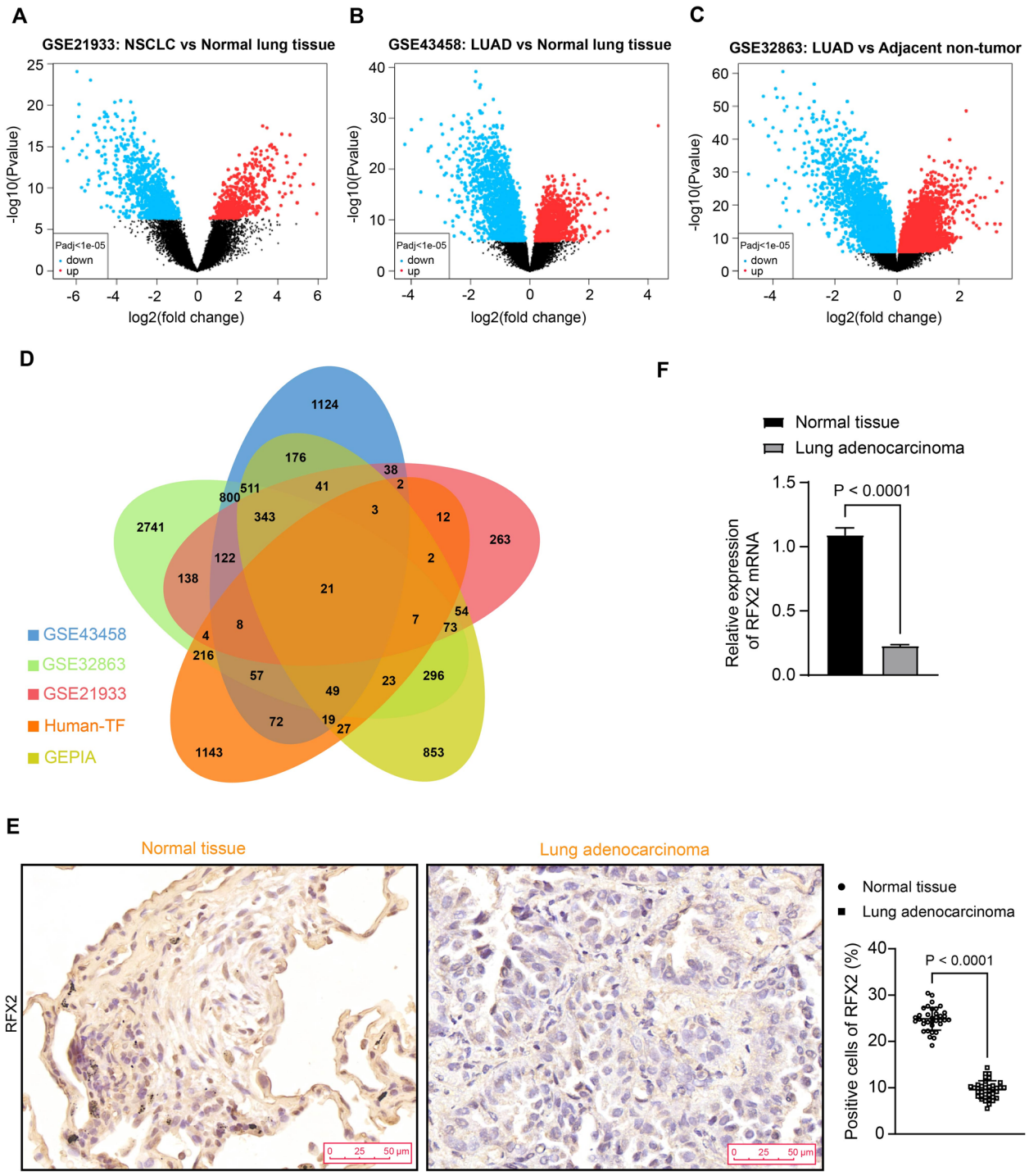

Fig. 1 Overexpression of RFX2 is identified in LUAD. **A** DEGs between 21 cases of NSCLC tissues and paired normal lung tissues in the GSE21933 dataset; **B** DEGs between tumor tissues of 80 LUAD patients who were smokers or non-smokers and normal lung tissues of those who never smoked in the GSE43458 dataset; **C** DEGs between 58 LUAD tissue and adjacent non-tumor tissue in the GSE32863 dataset; **D** Intersection of DEGs from GSE32863, GSE43458, and GSE21933 datasets, the first 2500 DEGs of LUAD in GEPIA, and human transcription factors obtained by Jvenn; **E** RFX2 expression in LUAD tissues and adjacent normal tissues was determined by IHC (n = 36); F, mRNA levels of RFX2 in LUAD tissue and adjacent normal tissue were determined by RT-qPCR (n = 36). Comparisons between 2 groups of a single factor were performed by t-test (EF)

downregulated in LUAD, but whether it is involved in LUAD progression is unknown.

RFX2 overexpression activates CD8$^+$ T cells and inhibits LUAD cell immune escape and malignant phenotype

Analysis by TIMER2.0 (http://timer.cistrome.org/) revealed that RFX2 was significantly and positively correlated with CD8$^+$ T cells in LUAD, yet not significantly correlated with CD8$^+$ T cells in lung squamous cell carcinoma (LUSC) (Fig. 2A). This may be due to the specificity of RFX2 for tumor immunity in LUAD, so we focused on immune escape in LUAD. We speculated whether LUAD progression was caused by the decrease of CD8$^+$ T cell infiltration due to the low expression of RFX2, which prompted immune escape.

To investigate the functional role of RFX2 in LUAD cells, we first measured RFX2 levels in BEAS-2B normal lung cells and A-549, NCI-H358, Calu-3, and H1975 LUAD cell lines (Fig. 2B). RFX2 was lowly expressed in LUAD cell lines, and we chose the A-549 and NCI-H358 cell lines with the lowest RFX2 expression for further study. RFX2 was overexpressed in A-549 and NCI-H358 cell lines through lentiviral infection, and oe-RFX2 efficiency was detected by RT-qPCR in both cell lines (Fig. 2C). WB analysis confirmed significantly enhanced RFX2 expression in A-549 and NCI-H358 cells in the oe-RFX2 group compared with the oe-NC group (Fig. 2D).

To elucidate whether RFX2 promotion of immune escape in LUAD cells is mediated by CD8$^+$ T cells, we co-cultured A-549 and NCI-H358 cells infected with oe-NC and oe-RFX2 with activated CD8$^+$ T cells, respectively. The contents of IFN-γ, GZMB, and PRF1 released by CD8$^+$ T cells in the co-culture system were detected by ELISA. IFN-γ, GZMB, and PRF1 were higher in the oe-RFX2 group (Fig. 2E). PD-L1 was lower in the cells of the oe-RFX2 group (Fig. 2F), indicating that the immune escape of LUAD cells was inhibited. CCK-8 showed that RFX2 overexpression notably hindered the viability of A-549 and NCI-H358 cells (Fig. 2G). The invasive ability of the cells was also reduced after RFX2 overexpression (Fig. 2H). However, the apoptosis of LUAD cells was strengthened upon RFX2 overexpression (Fig. 2I).

RFX2 directly activates RASSF1 transcription by binding to the RASSF1 promoter region

To further explore the downstream molecular regulatory mechanisms of transcription factor RFX2 in LUAD, we first downloaded the top 50 downstream targets of RFX2 from hTFtarget (http://bioinfo.life.hust.edu.cn/hTFtarget/#!/) and obtained only 1 intersection RASSF1 (Fig. 3A) with the DEGs in the GSE32863, GSE43458, GSE21933 datasets and the top 2500 DEGs of LUAD in GEPIA by Jvenn with a threshold of P adj < 1e-05. Although existing studies report the role of RASSF1 in lung cancer [16, 17], there is no investigation regarding the role of RASSF1 in the immune escape of LUAD. Therefore, we found that RASSF1 was also significantly positively correlated with the infiltration of CD8$^+$ T cells by TIMER2.0 analysis (Fig. 3B). Moreover, RASSF1 was significantly reduced in the datasets GSE32863 (LogFC = − 0.0508), GSE43458 (LogFC = − 0.2691704), and GSE21933 (LogFC = − 1.3123227). Proteomic analysis in UALCAN revealed that RFX2 was significantly downregulated in LUAD (Fig. 3C). hTFtarget prediction showed that RASSF1 was a downstream target of RFX2 (Fig. 3D). In addition, GEPIA correlation analysis showed a significant positive correlation between RFX2 and RASSF1 (Fig. 3E). IHC experiments showed that IHC staining of RASSF1 was significantly reduced in LUAD tissues (Fig. 3F). There was a significant positive correlation between protein expression of RFX2 and RASSF1 in our cohort (n = 36) (Fig. 3G). Luciferase reporter assay showed that the relative luciferase activity of the RASSF1 promoter luciferase reporter plasmid was substantially elevated after transfection of RFX2 overexpression plasmid in A-549 and NCI-H358 cells (Fig. 3H). RFX2 overexpression also increased the mRNA expression of RASSF1 in A-549 and NCI-H358 cells (Fig. 3I). Thus, RASSF1 was identified as the most likely transcription factor interacting with RFX2. In addition, ChIP assay results indicated that RFX2 was markedly enriched in the RASSF1 promoter in LUAD cells (Fig. 3J). Taken together, in LUAD, RFX2 can directly activate RASSF1 transcription by binding to the RASSF1 promoter region.

Silencing of RASSF1 abates the anti-tumor effects of RFX2 overexpression in vitro and in vivo

To confirm the effect of RFX2-regulated transcription of RASSF1 on LUAD progression, we infected A-549 and NCI-H358 cells with oe-RFX2 vector + sh-RASSF1 or sh-NC. RT-qPCR confirmed the successful regression of RASSF1 expression in the presence of overexpression of RFX2 overexpression (Fig. 4A). The ability of RFX2 overexpression to inhibit cell proliferation and invasion could be reversed by knocking down RASSF1 (Fig. 4B, C). In addition, the pro-apoptotic properties of RFX2 overexpression were also overturned by RASSF1 knockdown (Fig. 4D).

In addition, an in vivo tumor model was constructed by subcutaneous injection of LA-795 cells with stable overexpression of RFX2 (oe-NC as control) versus overexpression of RFX2 + sh-RASSF1 (oe-RFX2 + sh-NC as control) into C57BL/6 mice. The growth of tumors in the oe-RFX2 group was inhibited, whereas sh-RASSF1 promoted tumor growth (Fig. 4E, F). IHC detection of RFX2 and RASSF1 expression in tumor tissues (Fig. 4G)

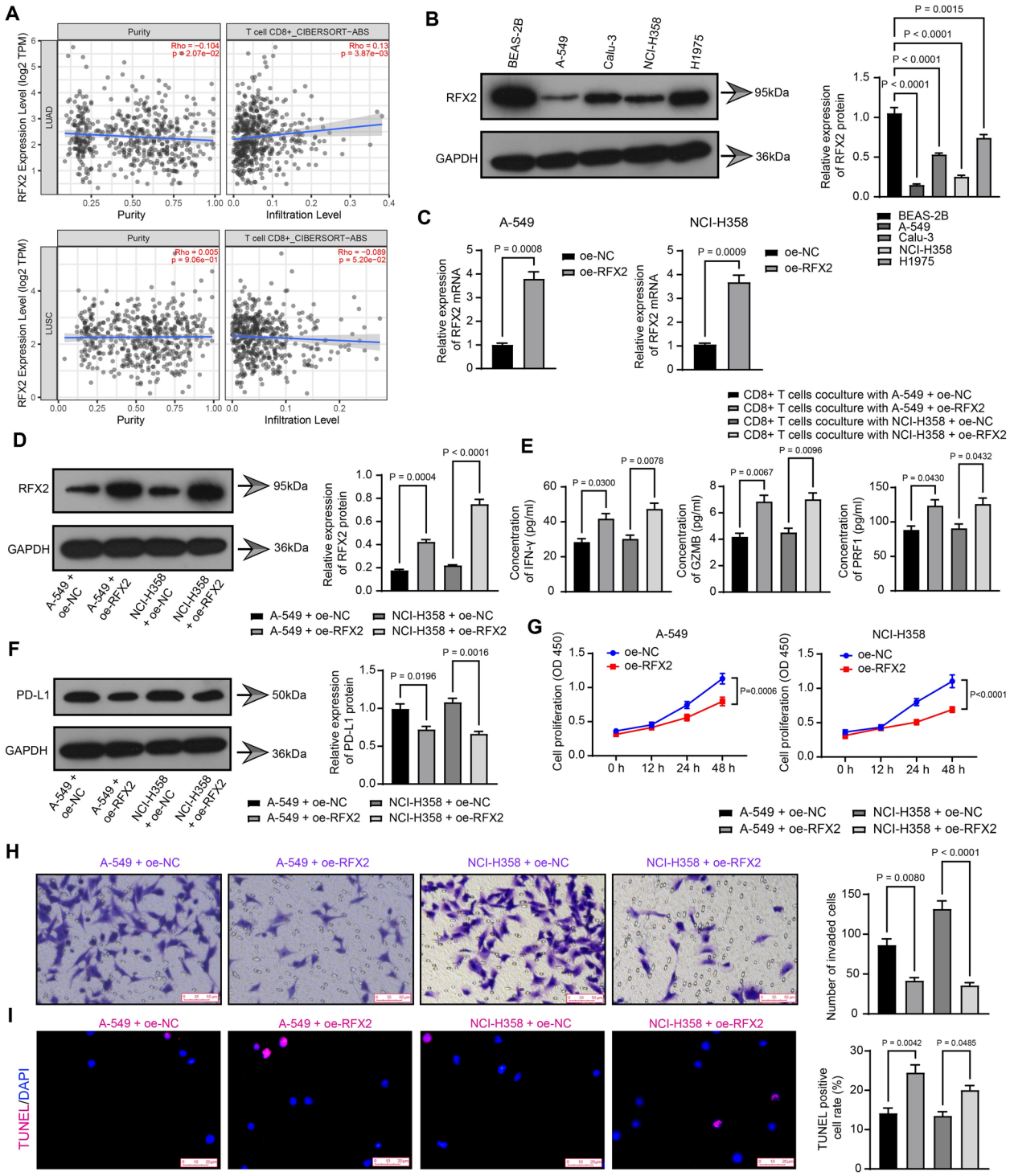

Fig. 2 RFX2 overexpression induces CD8$^+$ T cell activation and inhibits LUAD cell immune escape and malignant phenotype. **A** RFX2 expression correlates with the infiltration of CD8$^+$ T cells in LUAD and LUSC, respectively; **B** WB analysis of RFX2 protein expression in normal lung cells and LUAD cell lines; **C** RT-qPCR to detect oe-RFX2 efficiency in A-549 and NCI-H358 cells; **D** WB analysis of RFX2 protein expression in A-549 and NCI-H358 cells in the oe-NC and oe-RFX2 groups; **E** ELISA for IFN-γ, GZMB, and PRF1 contents in the oe-NC and oe-RFX2 groups; **F** WB analysis of PD-L1 expression in cells of the oe-NC and oe-RFX2 groups; **G** CCK8 assay for A-549 and NCI-H358 cell proliferation ability; **H** Transwell assay for invasion of A-549 and NCI-H358 cells overexpressing RFX2; **I** TUNEL assay for apoptosis of A-549 and NCI-H358 cells overexpressing RFX2. All cellular experiments were independently repeated 3 times. Comparisons between 2 groups of a single factor were performed by unpaired t-test (**C**); comparisons among multiple groups of a single factor were performed by one-way ANOVA (BDEFHI); comparisons among multiple groups of two factors were performed by two-way ANOVA (**G**)

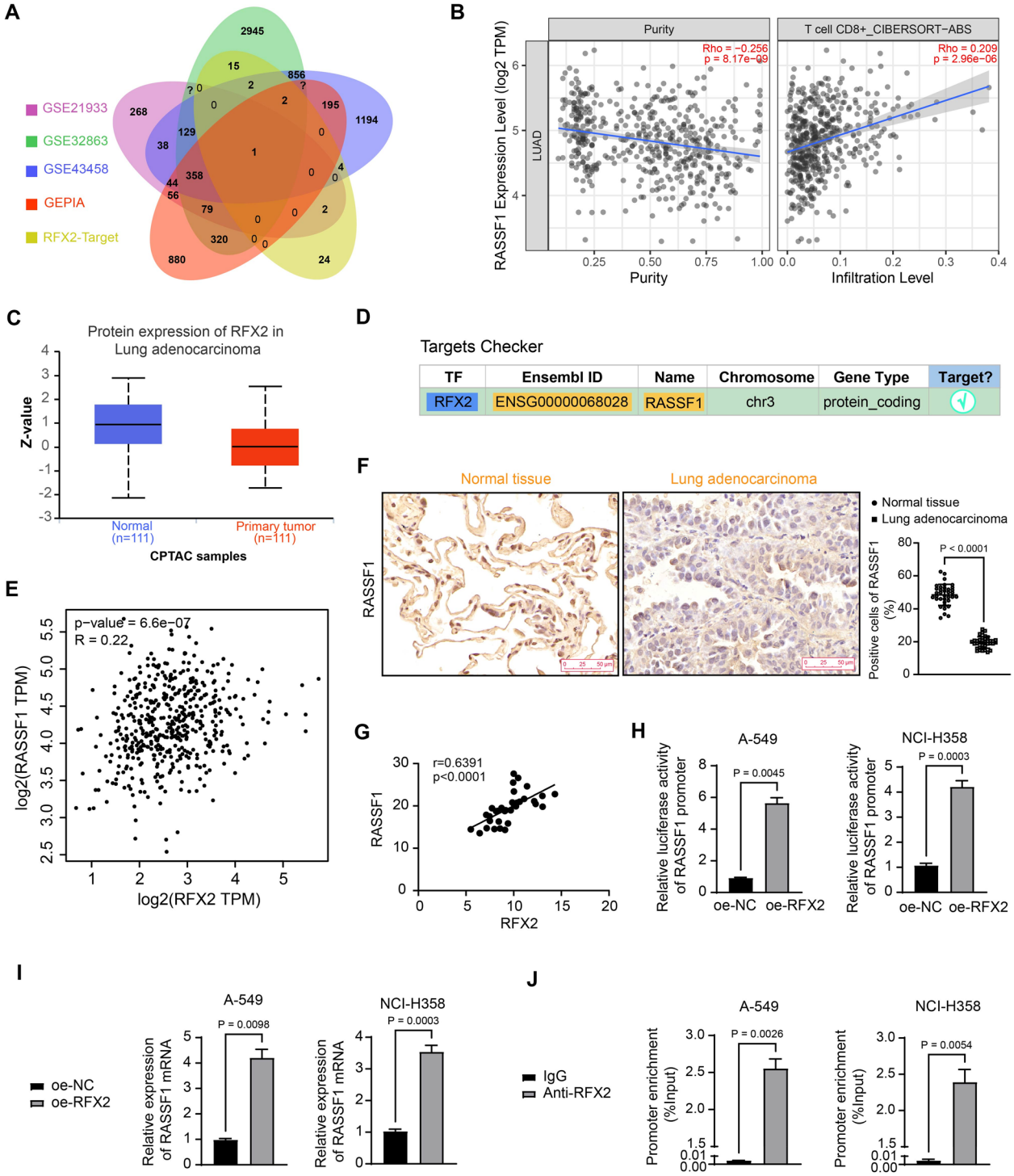

Fig. 3 Low RFX2 expression downregulates the expression of the downstream target RASSF1. **A** Intersection of DEGs of GSE32863, GSE43458, GSE21933 datasets, top 50 targets of RFX2 and the first 2500 DEGs of LUAD in GEPIA obtained by Jvenn; **B** TIMER2.0 analysis of the correlation between RASSF1 and the infiltration of $CD8^+$ T cells; **C** Proteomics analysis of RFX2 in LUAD by proteomics in UALCAN; **D** hTFtarget prediction of RFX2 downstream targets; **E** GEPIA correlation analysis of RFX2 with RASSF1; **F** IHC experiments to analyze RASSF1 expression in clinical LUAD tissue samples; **G** Correlation between RFX2 and RASSF1 protein expression; **H** Dual-luciferase assay confirmed the correlation between interaction between RFX2 and the RASSF1 promoter in A-549 and NCI-H358 cells; **I** RT-qPCR to detect mRNA expression of RASSF1 in the oe-NC and oe-RFX2 groups; **J** ChIP assay verified that RFX2 could bind to RASSF1 promoter in A-549 and NCI-H358 cells. All cell experiments were independently repeated 3 times. Single-factor comparison between the 2 groups was performed by t-test (FHIJ)

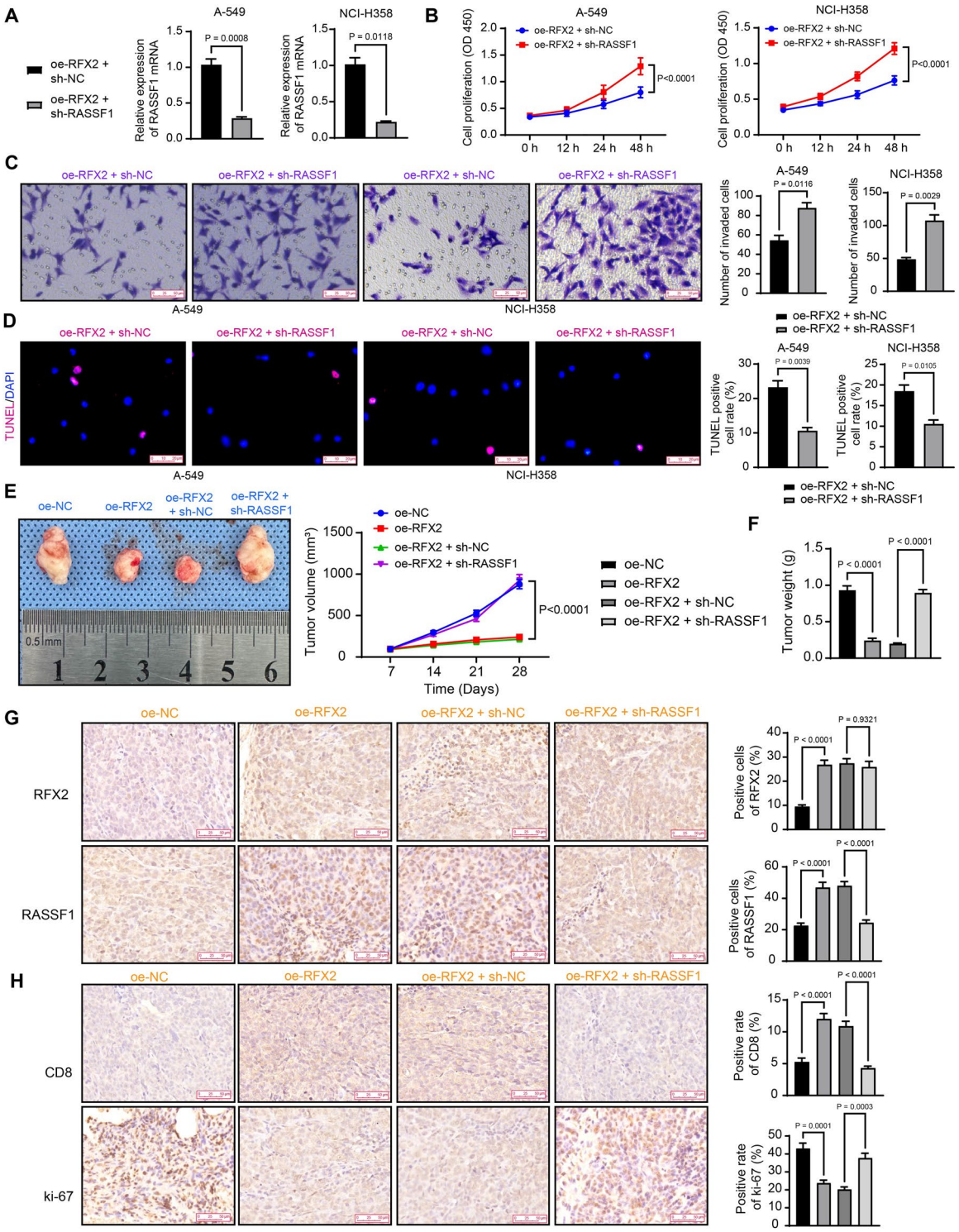

Fig. 4 RFX2 regulates RASSF1 transcription in LUAD progression. **A** mRNA expression of RASSF1 detected by RT-qPCR; **B** Proliferative ability of A-549 and NCI-H358 cells assessed by CCK-8 assay; **C** Invasive ability of A-549 and NCI-H358 cells determined by Transwell assay; **D** Apoptosis of A-549 and NCI-H358 cells determined by TUNEL assay; **E** Tumor volume analysis to assess the effect of overexpression of RFX2 and knockdown of RASSF1 on tumor growth; **F** Weight of tumors formed by LA-795 mouse LUAD cells; **G** RFX2 and RASSF1 expression in mouse transplanted tumor tissues detected by IHC; **H** CD8 and Ki-67 expression in transplanted tumor tissues detected by immunohistochemistry. All cellular experiments were independently repeated 3 times, and all animal experiments had 5 mice in each group. Unpaired t-test (ACD) was used for the comparison between 2 groups of a single factor, one-way ANOVA (FGH) for the comparison among multiple groups of a single factor, and two-way ANOVA (BE) for the comparison between 2 groups of two factors

confirmed the successful modeling. In addition, IHC revealed that the oe-RFX2 repressed Ki-67 while elevated CD8 expression in the tumor tissues. However, further RASSF1 knockdown upregulated Ki-67 in tumor tissues and reduced the $CD8^+$ T cell infiltration within the transplanted tumor was significantly downregulated (Fig. 4H).

RFX2/RASSF1 axis affects the Hippo pathway

RASSF1 can inhibit tumorigenesis in gastric cancer by activating the phosphorylation of YAP, thereby affecting the Hippo pathway [11]. The Hippo pathway is closely related to immune evasion in human cancer [18]. In addition, we analyzed the relationship between the Hippo signaling pathway and RASSF1 in the KEGG pathway database (https://www.kegg.jp/kegg/pathway.html). As shown in Fig. 5A, RASSF1 inhibits Hippo signaling through activation of Mst1/2 and Lats1/2 cascades to promote YAP/TAZ phosphorylation, thereby inhibiting Hippo signaling. Therefore, we further hypothesized that the significantly low expression of RFX2 in LUAD downregulated the expression of RASSF1, which in turn promoted immune escape in LUAD by reducing the phosphorylation of YAP.

We then determined the effect of the RFX2/RASSF1 axis on Hippo signaling. YAP expression was higher in A-549 and NCI-H358 cells than in BEAS-2B cells by WB analysis, while phosphorylated protein expression of YAP was decreased in A-549 and NCI-H358 cells (Fig. 5B). WB analysis revealed that RFX2 overexpression decreased YAP expression and promoted its phosphorylation, whereas the addition of sh-RASSF1 reversed the expression of YAP and its phosphorylation (Fig. 5C).

YAP activator reverses the inhibitory effect of RFX2 overexpression on LUAD cells

PY-60 was selected as a YAP activator to detect its effect on the Hippo pathway. The oe-RFX2 + DMSO and oe-RFX2 + PY-60 groups were set up. WB analysis revealed that compared to the oe-RFX2 + DMSO group, the protein level of YAP was elevated in the oe-RFX2 + PY-60 group, and YAP phosphorylation was inhibited (Fig. 6A). CCK-8 and Transwell assays evinced that the viability and invasive abilities of cells in the oe-RFX2 + PY-60 group were enhanced (Fig. 6B, C). By contrast, the TUNEL-positive cells were partially lost after the combined treatment of PY-60 (Fig. 6D). RT-qPCR detected higher mRNA expression of PD-L1 in the cells of the oe-RFX2 + PY-60 group (Fig. 6E), indicating immune escape of LUAD cells was induced. A-549 and NCI-H358 cells treated with DMSO and PY-60, respectively after RFX2 overexpression were co-cultured with $CD8^+$T cells. Low levels of IFN-γ, GZMB, and PRF1 were detected by ELISA in the co-culture system of the oe-RFX2 + PY-60 group (Fig. 6F).

Discussion

Based on morphological features, lung cancer has been historically classified as small cell lung cancer and NSCLC (75%), the latter including LUAD (60%), LUSC (30%), and other less common subtypes (10%) [19]. Given that the innate immune system plays an important role in tumor surveillance, therapeutic interventions for lung cancer should consider the known beneficial role of tackling the dynamic and complex interplay between cancer and immunity through successful immune surveillance and immune evasion prevention [20]. The present study was to reveal the effects of RXF2 on the immune escape of LUAD.

RFX1 overexpression has been reported to inhibit the tumor growth of hepatocellular carcinoma cells in vivo [21]. Similarly, we found here that RFX2 was poorly expressed in LUAD cell lines. Low-risk LUAD patients have higher immune cell infiltration states, especially $CD8^+$ T cells [22]. The RFX transcription factor complex cooperates with NOD-, LRR- and CARD-containing 5 to induce major histocompatibility complex class I gene expression, which plays a pivotal role in $CD8^+$ T cell activation and host adaptive-immune response [23]. Our results demonstrated that the levels of IFN-γ, GZMB, and PRF1 were raised in the co-culture system of LUAD cells with RFX2 overexpression and $CD8^+$ T cells, whereas PD-L1 expression was decreased. What is more, RFX2 overexpression impeded the viability and invasion and enhanced apoptosis of LUAD cells. These results and previous findings illustrated that RFX2 upregulation could contribute to the suppression of immune escape, proliferation, and invasion of LUAD cells. However, deleting genes encoding RNF2 in syngeneic murine models of triple-negative breast cancer was sufficient to induce durable tumor rejection and establish immune memory by enhancing infiltration and activation of NK and $CD4^+$ T-cells [24]. The paradoxical function has yet to be elucidated and might be partly attributed to different tumor microenvironments.

We have identified RASSF1 as a downstream target of RFX2 in LUAD. Low RASSF1 expression is associated with a growth advantage and immortalization of tumor cells and promoter hypermethylation of RASSF1 is considered a frequent event in lung cancer [10]. Our results further displayed that RFX2 was positively correlated with RASSF1 and could activate RASSF1 transcription by binding to the promoter region of RASSF1 in LUAD. RASSF1 is reported to be downregulated in non-small cell lung cancer, which is implicated in cell-cycle

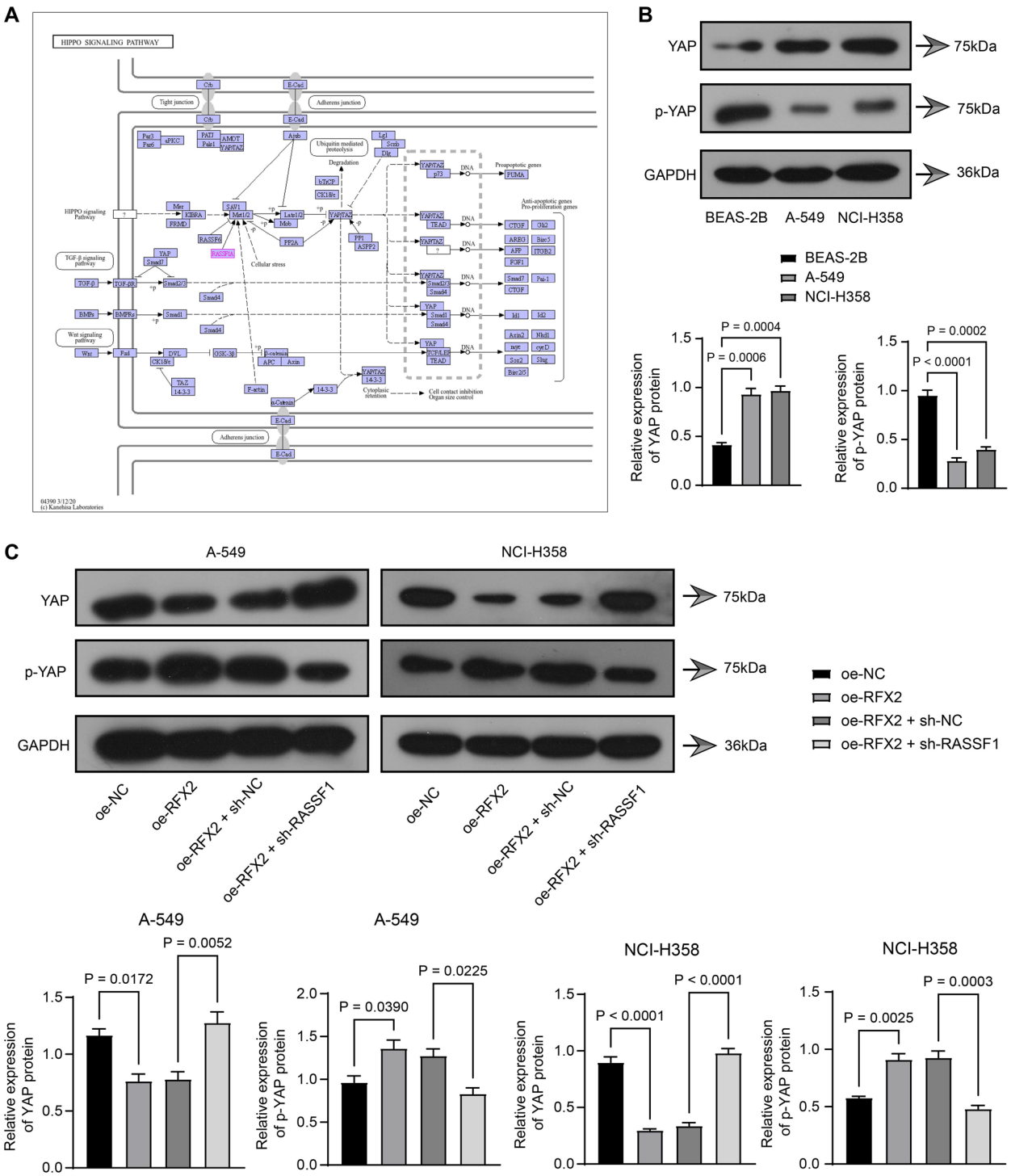

Fig. 5 RFX2/RASSF1 axis activates the Hippo pathway. **A** Localization of RASSF1 in Hippo signaling cascades analyzed using the KEGG pathway database; **B** Expression of YAP and its phosphorylated proteins in A-549 and NCI-H358 cells were analyzed by WB; **C** Expression of YAP and its phosphorylated proteins in the oe-NC, oe-RFX2, oe-RFX2 + sh-NC, and oe-RFX2 + sh-RASSF1 groups were analyzed by WB. All cellular experiments were independently repeated 3 times. Single-factor comparisons among multiple groups were performed by one-way ANOVA (BC)

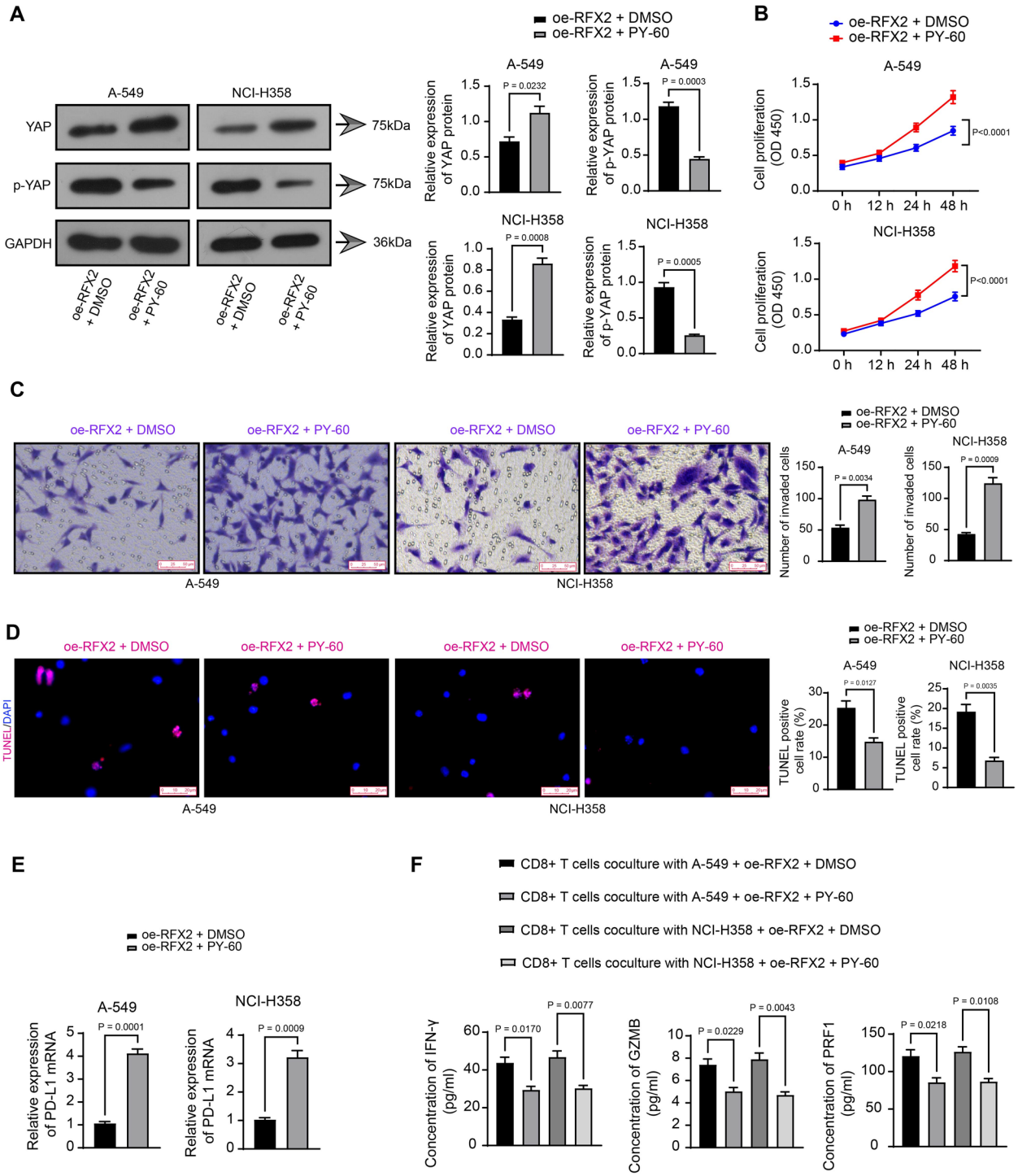

Fig. 6 YAP activator reverses the inhibitory effect of overexpression of RFX2 on LUAD cells. **A** WB analysis of YAP protein expression and its phosphorylation after addition of PY-60 in A-549 and NCI-H358 cells; **B** CCK-8 assay for cell viability; **C** Transwell assay for cell invasion; **D** TUNEL assay for cell apoptosis; **E** RT-qPCR analysis of PD-L1 mRNA expression; **F** ELISA to detect the levels of IFN-γ, GZMB, and PRF1. All cellular experiments were independently repeated 3 times. Comparisons between 2 groups of a single factor were performed by unpaired t-test (ACDE); comparisons among multiple groups of a single factor were performed by one-way ANOVA (**F**); comparisons between 2 groups of two factors were performed by two-way ANOVA (**B**)

regulation and apoptosis [25]. In mouse models, RFX2 overexpression inhibited the expression of Ki-67, a proliferation marker, and elevated CD8 expression, while RASSF1 knockdown led to the opposite results. Collectively, RFX2 could affect the anti-tumor immunity of $CD8^+$ T cells and participate in LUAD cell proliferation and invasion by regulating RASSF1 transcription.

RASSF1A has been identified as a critical upstream modifier of the core Hippo pathway [26]. Pasteurella multocida activates the Hippo-Yap pathway by inducing RASSF1 expression, and knockdown of RASSF1 significantly enhanced YAP activity and reduced apoptosis in the lung epithelial cell line [27]. Our results suggested that total YAP was upregulated while YAP phosphorylation was downregulated in LUAD cells. After RFX2 overexpression, YAP expression was reduced and YAP phosphorylation was restored, while RASSF1 silencing abrogated these changes. More specifically, RFX2 could affect the Hippo pathway by downregulating RASSF1 to repress YAP phosphorylation. The Hippo pathway is a master regulator of cell proliferation, and the alteration of the Hippo pathway results in cell invasion, migration, disease progression, and therapy resistance in cancers [28]. The combination of RFX2 overexpression and PY60 contributed to stronger viability and invasion of LUAD cells. In addition, YAP is expressed in activated $CD8^+$ T cells and YAP-deficient cells could produce more IFN-γ [29]. The activation of the tumor-intrinsic Hippo pathway shows a positive correlation with the abundance of $CD8^+$ T lymphocytes in mouse tumors and patients, whereas the blockade of the Hippo pathway effector YAP/TEAD potently improves antitumor immunity [30]. Our results showed that PD-L1 mRNA expression was enhanced while IFN-γ, GZMB, and PRF1 levels were lowered in LUAD cells treated with PY-60, which further indicated that the addition of a YAP activator after RFX2 overexpression could stimulate the proliferation, invasion, and immune escape of LUAD cells.

Taken together, RFX2 is weakly expressed in LUAD, downregulates RASSF1, and decreases YAP phosphorylation, thus promoting the immune escape of LUAD via the Hippo pathway (Fig. 7). Our findings provide new insights for understanding the molecular mechanisms of LUAD and delineate a potential therapeutic strategy for inhibiting the immune escape of LUAD cells and improving the prognosis of LUAD patients.

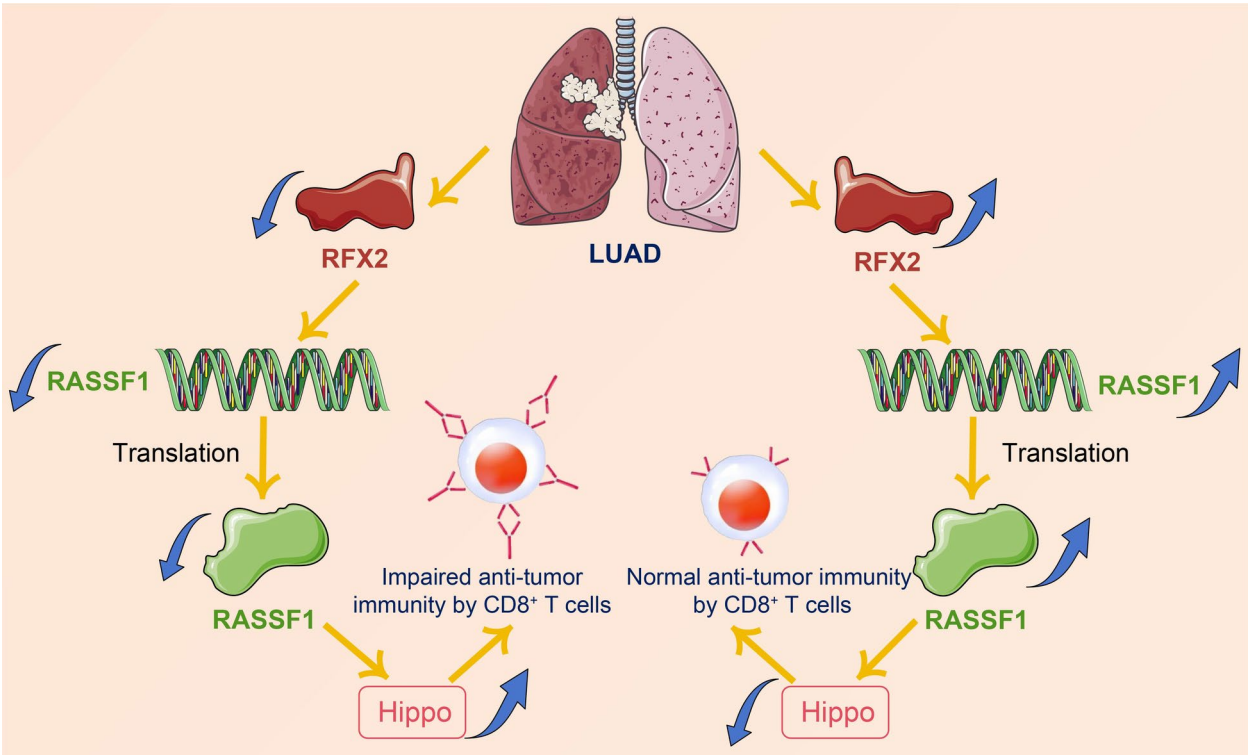

Fig. 7 Graphical abstract. Significantly low RFX2 expression in LUAD led to downregulation of RASSF1 levels, which in turn activated Hippo signaling and promoted immune escape in LUAD by impairing anti-tumor immunity of $CD8^+$ T cells

Materials and methods

Ethical statement

All patients or their guardians signed an informed consent form before participating in the study. The study followed the principles of the *Declaration of Helsinki* and the protocol was approved by the Medical Ethics Committee of Wujin Hospital Affiliated with Jiangsu University. All animal experiments were approved by the Animal Ethics Committee of Wujin Hospital Affiliated with Jiangsu University and were performed according to animal ethics guidelines.

Dataset collection and processing

The GSE21933, GSE43458, and GSE32863 datasets were downloaded from the GEO database (https://www.ncbi.nlm.nih.gov/gds/?term=), and the two groups (tumor samples and control samples) were compared to identify the DEGs using GEO2R analysis. Specifically, we clicked "Define groups", assigned the tumor samples and control samples into two groups in sequential order, and adjusted the *p*-values using Benjamini & Hochberg and the significance level cut-off to 0.00001 from "Options". After analysis, the DEGs were downloaded and presented in the form of tables and volcano diagrams.

"Cancer Type Analysis" on the homepage of GEPIA was used to perform differential expression analysis. In brief, LUAD in the "Dataset" column and Both in the "Chromosomal Distribution" column were selected. The list was ranked according to the value of adj *p* from smallest to largest. Finally, the top 2500 genes with the smallest adj *p* were downloaded as the research objects. From the HumanTFDB homepage, the human TFs were downloaded after clicking "human TF list download". Jvenn (https://jvenn.toulouse.inrae.fr/app/example.html) is a JQuery plugin based on J.C Oliveros' venny tool which can filter elements common to the highest 6 listed data based on the input list data and present them in a Venn diagram.

The DEGs of GSE21933, GSE43458, and GSE32863 conditional on *p* adj < 0.00001, the first 2500 DEGs of the LUAD in GEPIA, and the human TFs were integrated to obtain 21 shared intersections via Jvenn, followed by further screening using the Kaplan–Meier Plotter tool. Specifically, "Use multiple genes" was clicked after "Start KM Plotter for lung cancer" to enter the Gene Symbol of the 21 intersecting genes. "Start analysis using selected probes" was used to include the 21 intersected genes in the analysis of the OS of lung cancer patients.

TIMER 2.0 (http://timer.cistrome.org/) is a comprehensive database for analyzing immune infiltration in different cancer types. Under "Immune Association", RFX2 or RASSF1 were entered in the "Gene Expression" column, and T cell $CD8^+$ in the "Immune Infiltrates" column was selected to explore the correlation between gene expression and $CD8^+$ CIBERSORT-ABS infiltration in LUSC and LUAD.

hTFtarget (http://bioinfo.life.hust.edu.cn/hTFtarget/#!/) was used to predict possible target genes of RFX2. RFX2 was entered in the "TF" column on the homepage and Details in "General targets" was clicked to download the top 50 predicted target genes.

The top 50 target genes of RFX2 were combined with the DEGs of GSE32863, GSE43458, and GSE21933 and the top 2,500 DEGs of LUAD in GEPIA in Jvenn. The expression of RFX2 protein in LUAD was analyzed using the Proteomics database of UALCAN (https://ualcan.path.uab.edu/). The correlation analysis tool in the multiple gene comparison section of GEPIA was further used to analyze the Spearman correlation between RFX2 and RASSF1 in LUAD tumors.

Cell culture

Human LUAD cells A-549 (SNL-089), NCI-H358 (SNL-392), Calu-3 (SNL-214), H1975 (SNL-087), and mouse LUAD cells LA-795 (SNL-351), as well as normal lung cell line BEAS-2B (SNL-203) were purchased from Suncell (Wuhan, Hubei, China). All cells were cultured in complete DMEM (Gibco, Grand Island, NY, USA) supplemented with 10% fetal bovine serum (Sigma-Aldrich, St. Louis, MO, USA), penicillin/streptomycin (Sigma-Aldrich), and L-glutamine (Sigma-Aldrich) with 5% CO_2 at 37 °C under humid conditions. Cells were infected with overexpression lentivirus oe-RFX2, shRNA lentivirus sh-RASSF1, and control viruses (viral titer of 10^8 TU/mL) (from Vector Builder, Guangzhou, Guangdong, China) for puromycin selection (5 μg/mL) to obtain stably transfected cells.

A-549 and NCI-H358 cells were seeded in 6-well plates in complete DMEM at 5×10^5 per well. The next day, cells were treated with PY-60 (10 μM, SML3740-5MG, Sigma-Aldrich) or DMSO for another 24 h. Cells were collected by centrifugation at 300 *g* for 3 min [31].

Clinical specimens

Thirty-six samples from LUAD patients were collected at Wujin Hospital Affiliated with Jiangsu University from 2021 to 2023. Liquid nitrogen-frozen LUAD tissues, paracancerous tissues, and corresponding paraffin-embedded specimens were collected. No patients had received any systemic therapy before sample collection. The general and clinical characteristics of the study participants are listed in Table 1.

Table 1 Clinical information of included patients

Clinical features	Patient number (n = 36)
Age	
≤ 60 years	11
> 60 years	25
Sex	
Female	16
Male	20
Metastasis stage	
M0	29
M1	7
TNM stage	
Stage I	7
Stage II	9
Stage III	13
Stage IV	7
N stage	
N0	12
N1	16
N2	5
N3	3

Table 2 Primer sequences for PCR

Gene	Forward Sequence (5′-3′)	Reverse Sequence (5′-3′)
RFX2	CTGCGACCACATCCTCTACCAG	GCTCTTGGCAAAGTTACG GATGG
RASSF1	AGTGGGAGACACCTGACC TTTC	GAAGCCTGTGTAAGAACCGTCC
PD-L1	TGCCGACTACAAGCGAAT TACTG	CTGCTTGTCCAGATGACTTCGG
GAPDH	GTCTCCTCTGACTTCAAC AGCG	ACCACCCTGTTGCTGTAGCCAA

RFX regulatory factor X, *RASSF1* RAS-association domain family 1, *PD-L1* programmed cell death 1 ligand 1, *GAPDH* glyceraldehyde-3-phosphate dehydrogenase

Establishment of mouse graft tumor models

Male C57BL/6 mice (10–20 g) were purchased from Vital River (Beijing, China). Twenty mice were randomized into 4 groups of 5 mice each: oe-NC, oe-RFX2, oe-RFX2 + sh-NC, and oe-RFX2 + sh-RASSF1 groups. The mice were randomly housed with food and water. Then 2.0×10^6 LA-795 cells were inoculated in 100 μL DMEM and given to male mice for subcutaneous injection on the right side. One week from the injection of tumor cells, the tumor volume was tracked using calipers and calculated [(length × width^2)/2], and the weekly volume was recorded for each mouse. After 4 weeks, the tumor weight after tumor resection was measured after mice were euthanized by intraperitoneal injection of an overdose of sodium pentobarbital (150 mg/kg).

IHC

Tumor specimens were fixed in 10% formalin for 72 h, paraffin-embedded, and cut into 4 μm sections. Sections were stained according to the manufacturer's instructions with Anti-RFX2 (1/200, orb769915, Biorbyt Ltd, Cambridge, UK), Anti-RASSF1 (1/50, abx212287, Abbexa Ltd., Cambridge, UK), Anti-CD8 alpha (1/2000, ab217344, Abcam Inc., Cambridge, MA, USA) and Anti-Ki-67 (1/150; MA5-14,520, Thermo Fisher, Waltham, MA, USA). Sections were incubated overnight at 4 °C with primary antibodies and stained with goat anti-rabbit IgG H&L (1/30,000; ab205718; Abcam) coupled with horseradish peroxidase. Next, the sections were stained with the chromogenic agent diaminobenzidine (P0202, Beyotime, Shanghai, China), counterstained with hematoxylin, and dehydrated. All samples were examined independently by two pathologists.

Reverse transcription-quantitative polymerase chain reaction (RT-qPCR)

Total RNA from cells and tissues was extracted using TransZol Up (ET111-01-V2, TransGen Biotech, Beijing, China) and dissolved in DEPC-treated water. RNA concentration was measured by reading the optical density (OD) value at 260 nm using a microspectrophotometer. RNA purity was verified by OD260/OD280, and 28S/18S was measured by gel electrophoresis to assess RNA integrity. Concentration of all RNA samples > 0.5 μg/μL; RNA integrity number > 8.0, 28S/18S ≥ 1.8; OD260/OD280 = 1.9–2.0. After reverse transcription using the PrimeScript RT kit (RR047Q, Takara, Tokyo, Japan), SYBR Premix Ex Taq II (RR820A, Takara) was used according to the manufacturer's instructions for RT-qPCR. Using GAPDH as a reference [32], the relative expression levels were calculated using the $2^{-\Delta\Delta Ct}$ method. The primer sequences are shown in Table 2.

Western blot (WB)

Total proteins were extracted using RIPA buffer (89,901, Gibco) containing PMSF (ST505, Beyotime) and quantified using the BCA protein assay kit (ab102536, Abcam). Protein samples (30 μg) were separated by 10% SDS-PAGE, transferred to PVDF (ab133411,

Abcam) membranes, and incubated with RFX2 antibody (1/5000; NBP2-13224, Novus Biologicals), PD-L1 antibody (1/2000; NBP2-15791, Novus Biologicals), active YAP1 antibody [EPR19812] (1/1000; ab205270, Abcam), YAP1 (phospho S127) antibody [EP1675Y] (1/30,000, ab76252, Abcam), and GAPDH antibody (1/5000; ab8245, Abcam) overnight at 4 °C. After incubation with goat anti-rabbit IgG H&L (1/30,000; ab205718; Abcam) for 1 h at 37 °C, target proteins were visualized on PVDF membranes using the Pierce ECL kit (32,106, Solarbio, Beijing, China).

Cell co-culture

A-549 and NCI-H358 cells with or without PY-60 and DMSO treatment were maintained in DMEM as described above. Human primary $CD8^+$ cytotoxic T Cells (PCS-800-017, American Type Culture Collection, Manassas, VA, USA) were activated. CD3e monoclonal antibody (145-2C11) (5 μg/mL; 16-0031-82, eBioscience, San Diego, CA, USA) was pre-coated in 96-well plates at 4 °C overnight. Subsequently, CD28 monoclonal antibody (37.51) (1 μg/mL; 16–0281-82, eBioscience) was added to the plate. After activation, T cells were cultured in 24-well plates for 24 h in the presence of A-549 and NCI-H358 cells [33].

Enzyme-linked immunosorbent assay (ELISA)

INF-γ (EH249RBX10, Thermo Fisher), Perforin (PRF1, BMS2306, Thermo Fisher), and Granzyme B (GZMB) (BMS2027-2, Thermo Fisher) were measured according to the ELISA kit instructions. Total protein was isolated using pre-cooled PBS. Total protein was diluted 1:1 with sample dilution or non-diluted total protein. A volume of 100 μL of the sample was added to the ELISA plate and incubated at 37 °C for 90 min. After discarding the liquid, the samples were air-dried without washing. Biotinylated antibody working solution (concentrated biotinylated detection antibody: biotinylated detection antibody diluent = 1:100) was added for 60-min incubation at 37 °C. After washing three times, the coupler (Concentrated HRP Coupler: HRP Conjugate Diluent = 1:100) was added for 30-min incubation at 37 °C. After washing the plate five times, substrate reagent (TMB) was added for 15-min incubation with a fluorescent agent at 37 °C. The reaction was terminated by adding a termination solution. The optical density (OD) of each well was measured at 450 nm using a microplate marker (Bioteck, Winooski, VT, USA).

Cell viability assay

Cell viability was measured using the cell counting kit-8 (CCK-8) (CK04, Dojindo, Tokyo, Japan). Briefly, cells were seeded in 96-well plates at 3×10^3/well and incubated with 10 μL of CCK-8 for 1 h at 37 °C with 5% CO_2. The OD value was measured after 0, 12, 24, and 48 h. Cell proliferation was determined by OD values at 450 nm using a microplate reader.

TUNEL assay

A-549 and NCI-H358 cells with different treatments were tested for apoptosis by CoraLite 594 TUNEL Apoptosis Detection Kit (PF00009, ProteinTech Group, Chicago, IL, USA). Briefly, 4% paraformaldehyde solution was added to the cells and left at 4 °C for 30 min. The cells were permeabilized with PBS solution containing 0.2% Triton X-100 at room temperature for 20 min and incubated with 50 μL of TUNEL reaction solution containing 2 μL of TdT enzyme for 60 min at 37 °C in the dark and with 2 μg/mL of DAPI staining solution for 10 min at room temperature in the dark. TUNEL-positive staining was observed using fluorescence microscopy.

Transwell assay

The Transwell system (8 μm pore size, 3464, Corning Glass Works, Corning, N.Y., USA) was used for cell invasion assay. Cells were seeded in the upper chamber and cultured in a serum-free medium. The lower chamber was supplemented with serum medium, and the bottom of the upper chamber was coated with Matrigel. After 48 h, the cells on the upper surface were scrubbed off, and then the cells on the lower surface were fixed, stained, washed, and photographed for counting.

Dual-luciferase assay

A pGL3-based luciferase reporter vector (VT1554, Youbio, Hunan, China) containing the RASSF1 promoter along with the Renilla luciferase plasmid was transfected into A-549 and NCI-H358 cells stably overexpressing RFX2, as well as control cells, using Lipofectamine 3000 (L3000075, Thermo Fisher Scientific Inc.). After 48 h, luciferase activity was assayed by a dual-luciferase assay system, and firefly luciferase activity was normalized to Renilla activity.

Chromatin immunoprecipitation (ChIP)

SimpleChIP Plus Enzymatic ChIP Kit (Magnetic Beads) (#9005S, Cell Signaling Technology, Danvers, MA, USA) was used. Cells were fixed in 1% paraformaldehyde, harvested, and sonicated. A proportion of the sample (5%) was used as Input, and the remaining samples were incubated with Anti-RFX2 (1/20, NBP2-13224, Novus Biologicals) and IgG. Immunoprecipitated DNA was analyzed by RT-qPCR. ΔCt [normalized ChIP] = Ct [ChIP]–[Ct (Input)–log2(Input Dilution Factor)], %

Input = $2 - \Delta$Ct[normalized ChIP]), where Input Dilution factor = $0.05^{-1} = 20$.

Statistical analysis

Data were analyzed using Prism 8.0.2 statistical software (GraphPad Software, San Diego, CA, USA). All values are expressed as mean ± standard error of the mean (SEM). Comparisons between 2 groups were analyzed by t-test, comparisons among multiple groups were analyzed by one-way ANOVA, and comparisons among multiple groups with two factors were analyzed by two-way ANOVA. $P < 0.05$ was considered statistically significant. The cellular experiments were repeated three times independently, and the animal experiments had five mice in each group.

Supplementary Information

The online version contains supplementary material available at https://doi.org/10.1186/s13008-025-00147-z.

Supplementary material 1: Fig S1. The prognostic significance of 21 intersecting genes in lung cancer by Kaplan-Meier Plotter.

Supplementary material 2.

Author contributions

ZZK and YW contributed to the conception and design of the work, analyzed and interpreted the data, and drafted the manuscript. PZ, JHX, and YZ performed the experiments and analyzed the data. All authors read and approved the final manuscript.

Funding

None.

Availability of data and materials

No datasets were generated or analysed during the current study.

Declarations

Competing interests

The authors declare no competing interests.

Author details

[1]Department of Laboratory, Wujin Hospital Affiliated With Jiangsu University, No. 2 of Yongning North Road, Changzhou 213002, Jiangsu, People's Republic of China. [2]The Wujin Clinical College of Xuzhou Medical University, Xuzhou 221006, Jiangsu, People's Republic of China. [3]Department of Medical Laboratory, Xuzhou Mining Group General Hospital, Xuzhou 221011, Jiangsu, People's Republic of China.

Received: 16 October 2024 Accepted: 27 February 2025
Published online: 11 March 2025

References

1. Inamura K. Clinicopathological characteristics and mutations driving development of early lung adenocarcinoma: tumor initiation and progression. Int J Mol Sci. 2018;19(4):1259.
2. Nguyen TT, Lee HS, Burt BM, et al. A lepidic gene signature predicts patient prognosis and sensitivity to immunotherapy in lung adenocarcinoma. Genome Med. 2022;14(1):5.
3. Denisenko TV, Budkevich IN, Zhivotovsky B. Cell death-based treatment of lung adenocarcinoma. Cell Death Dis. 2018;9(2):117.
4. Song L, Gong Y, Wang E, Huang J, Li Y. Unraveling the tumor immune microenvironment of lung adenocarcinoma using single-cell RNA sequencing. Ther Adv Med Oncol. 2024;16:17588359231210274.
5. Tian Y, Zhai X, Yan W, Zhu H, Yu J. Clinical outcomes of immune checkpoint blockades and the underlying immune escape mechanisms in squamous and adenocarcinoma NSCLC. Cancer Med. 2021;10(1):3–14.
6. Sugiaman-Trapman D, Vitezic M, Jouhilahti EM, et al. Characterization of the human RFX transcription factor family by regulatory and target gene analysis. BMC Genomics. 2018;19(1):181.
7. Taniwaki M, Daigo Y, Ishikawa N, et al. Gene expression profiles of small-cell lung cancers: molecular signatures of lung cancer. Int J Oncol. 2006;29(3):567–75.
8. Zheng W, Zhang S, Guo H, et al. Multi-omics analysis of tumor angiogenesis characteristics and potential epigenetic regulation mechanisms in renal clear cell carcinoma. Cell Commun Signal. 2021;19(1):39.
9. Zinatizadeh MR, Momeni SA, Zarandi PK, et al. The role and function of ras-association domain family in cancer: a review. Genes Dis. 2019;6(4):378–84.
10. Walter RFH, Rozynek P, Casjens S, et al. Methylation of L1RE1, RARB, and RASSF1 function as possible biomarkers for the differential diagnosis of lung cancer. PLoS ONE. 2018;13(5): e0195716.
11. Kim SH, Jin H, Meng RY, et al. Activating hippo pathway via Rassf1 by ursolic acid suppresses the tumorigenesis of gastric cancer. Int J Mol Sci. 2019;20(19):4709.
12. He M, Zhou Z, Shah AA, et al. New insights into posttranslational modifications of Hippo pathway in carcinogenesis and therapeutics. Cell Div. 2016;11:4.
13. Kobayashi Y, Lim SO, Yamaguchi H. Oncogenic signaling pathways associated with immune evasion and resistance to immune checkpoint inhibitors in cancer. Semin Cancer Biol. 2020;65:51–64.
14. Madhi H, Lee JS, Choi YE, et al. FOXM1 inhibition enhances the therapeutic outcome of lung cancer immunotherapy by modulating PD-L1 expression and cell proliferation. Adv Sci. 2022;9(29): e2202702.
15. Merjaneh N, Hajjar M, Lan YW, Kalinichenko VV, Kalin TV. The promise of combination therapies with FOXM1 inhibitors for cancer treatment. Cancers. 2024;16(4):756.
16. Li N, Zeng Y, Huang J. Signaling pathways and clinical application of RASSF1A and SHOX2 in lung cancer. J Cancer Res Clin Oncol. 2020;146(6):1379–93.
17. Pankova D, Jiang Y, Chatzifrangkeskou M, et al. RASSF1A controls tissue stiffness and cancer stem-like cells in lung adenocarcinoma. EMBO J. 2019;38(13): e100532.
18. Xu C, Jin G, Wu H, et al. SIRPgamma-expressing cancer stem-like cells promote immune escape of lung cancer via Hippo signaling. J Clin Invest. 2022. https://doi.org/10.1172/JCI141797.
19. Mogavero A, Bironzo P, Righi L, et al. Deciphering lung adenocarcinoma heterogeneity: an overview of pathological and clinical features of rare subtypes. Life. 2023;13(6):1291.
20. Wu X, Gu Z, Chen Y, et al. Application of PD-1 blockade in cancer immunotherapy. Comput Struct Biotechnol J. 2019;17:661–74.
21. Su JC, Chiang HC, Tseng PH, et al. RFX-1-dependent activation of SHP-1 inhibits STAT3 signaling in hepatocellular carcinoma cells. Carcinogenesis. 2014;35(12):2807–14.
22. Song P, Li W, Guo L, et al. Identification and validation of a novel signature based on NK cell marker genes to predict prognosis and immunotherapy response in lung adenocarcinoma by integrated analysis of single-cell and bulk RNA-sequencing. Front Immunol. 2022;13:850745.
23. Meissner TB, Liu YJ, Lee KH, et al. NLRC5 cooperates with the RFX transcription factor complex to induce MHC class I gene expression. J Immunol. 2012;188(10):4951–8.
24. Zhang Z, Luo L, Xing C, et al. RNF2 ablation reprograms the tumor-immune microenvironment and stimulates durable NK and CD4(+) T-cell-dependent antitumor immunity. Nat Cancer. 2021;2(10):1018–38.
25. Korner A, Mudduluru G, Manegold C, Allgayer H. Enzastaurin inhibits invasion and metastasis in lung cancer by diverse molecules. Br J Cancer. 2010;103(6):802–11.
26. Yeung B, Yu J, Yang X. Roles of the Hippo pathway in lung development and tumorigenesis. Int J Cancer. 2016;138(3):533–9.

27. Zhao G, Tang Y, Liu X, et al. Pasteurella multocida activates Rassf1-Hippo-Yap pathway to induce pulmonary epithelial apoptosis. Vet Res. 2024;55(1):31.
28. Mohajan S, Jaiswal PK, Vatanmakarian M, et al. Hippo pathway: regulation, deregulation and potential therapeutic targets in cancer. Cancer Lett. 2021;507:112–23.
29. Lebid A, Chung L, Pardoll DM, Pan F. YAP attenuates CD8 T cell-mediated anti-tumor response. Front Immunol. 2020;11:580.
30. Peng L, Zhou L, Li H, et al. Hippo-signaling-controlled MHC class I antigen processing and presentation pathway potentiates antitumor immunity. Cell Rep. 2024;43(4):114003.
31. Grzelak EM, Elshan N, Shao S, et al. Pharmacological YAP activation promotes regenerative repair of cutaneous wounds. Proc Natl Acad Sci U S A. 2023;120(28): e2305085120.
32. Said HM, Polat B, Hagemann C, et al. Absence of GAPDH regulation in tumor-cells of different origin under hypoxic conditions in—vitro. BMC Res Notes. 2009;2:8.
33. Amit M, Xie T, Gleber-Netto FO, et al. Distinct immune signature predicts progression of vestibular schwannoma and unveils a possible viral etiology. J Exp Clin Cancer Res. 2022;41(1):292.

Publisher's Note